2010

Simulation of Macroscopic Deformation Using a Sub-particle DEM Approach

Leela Kempton
University of New South Wales

David J. Pinson
BlueScope Steel Limited, DavidJ.Pinson@bluescopesteel.com

Sheng Chew
BlueScope Steel Limited, shengc@uow.edu.au

Paul Zulli
University of Wollongong, paulz@uow.edu.au

Aibing Yu
University of New South Wales

Publication Details

Kempton, L., Pinson, D., Chew, S., Zulli, P. & Yu, A. (2010). Simulation of Macroscopic Deformation Using a Sub-particle DEM Approach. Chemeca 2010: Engineering at the Edge (pp. 1216-1226). Barton, Australia: Engineers Australia.

Simulation of Macroscopic Deformation Using a Sub-particle DEM Approach

Abstract
A limitation in numerical modelling of the ironmaking blast furnace is the lack of ability to quantify the effects of particle deformation and subsequent loss of porosity arising from the softening and melting of ferrous materials. Previous attempts to consider deformation focussed solely on the macroscopic effects such as resistance to gas flow, with an assumed decrease in porosity proportional to temperature. Instead, it is proposed to approximate particle scale deformation using a modified subparticle Discrete Element Method approach, where each 'ore' particle is represented using an agglomerate of discrete elements with temperature dependent properties. Cohesive forces binding the agglomerate were obtained from standard models (Linear Hysteretic and a simplified Hertz-JKR). This paper considers the limiting case of a two-particle agglomerate, in order to assess how physically realistic the behaviour is under external force conditions including uni-axial tension and rotation. Future work will extend this approach to larger scale agglomerates to simulate the shape change of materials as they undergo softening-melting.

Keywords
dem, simulation, approach, macroscopic, deformation, sub-particle

Disciplines
Engineering | Science and Technology Studies

Publication Details
Kempton, L., Pinson, D., Chew, S., Zulli, P. & Yu, A. (2010). Simulation of Macroscopic Deformation Using a Sub-particle DEM Approach. Chemeca 2010: Engineering at the Edge (pp. 1216-1226). Barton, Australia: Engineers Australia.

SIMULATION OF MACROSCOPIC DEFORMATION USING A SUB-PARTICLE DEM APPROACH

Leela Kempton[1], David Pinson[2], Sheng Chew[2], Paul Zulli[2] and Aibing Yu[1]

[1] School of Materials Science and Engineering, University of New South Wales, Sydney, NSW 2052, Australia

[2] BlueScope Steel Research, Port Kembla, NSW 2505, Australia.

ABSTRACT

A limitation in numerical modelling of the ironmaking blast furnace is the lack of ability to quantify the effects of particle deformation and subsequent loss of porosity arising from the softening and melting of ferrous materials. Previous attempts to consider deformation focussed solely on the macroscopic effects such as resistance to gas flow, with an assumed decrease in porosity proportional to temperature. Instead, it is proposed to approximate particle scale deformation using a modified subparticle Discrete Element Method approach, where each "ore" particle is represented using an agglomerate of discrete elements with temperature dependent properties. Cohesive forces binding the agglomerate were obtained from standard models (Linear Hysteretic and a simplified Hertz-JKR). This paper considers the limiting case of a two-particle agglomerate, in order to assess how physically realistic the behaviour is under external force conditions including uni-axial tension and rotation. Future work will extend this approach to larger scale agglomerates to simulate the shape change of materials as they undergo softening-melting.

Keywords: DEM, particle deformation, cohesive zone, blast furnace

INTRODUCTION

In the blast furnace, layers of ferrous materials and coke are charged alternately from the top, and are heated by gas as they descend through the furnace. As the ferrous materials undergo softening and melting, in an area known as the cohesive zone, a localised loss of porosity results in the ferrous layers, which in turn affects the gas flow through the furnace. Although little is understood of the mechanics of the cohesive zone, this process is known to be vital in controlling the production capability of the furnace. Numerical modelling, including computational fluid dynamics (CFD) as well as discrete element method (DEM) models have been used to simulate the conditions within the furnace and understand improvements that could be made. However, a limiting feature of models developed to date is the lack of ability to quantify the conditions within the cohesive zone; specifically, quantification of effects that deformation and subsequent loss of porosity have on the permeability to gas, liquid and powder flows.

Previous attempts to consider deformation effects in CFD models have focussed solely on macroscopic factors such as fluid flow and heat transfer, with an assumed decrease in porosity proportional to the temperature (Chew *et al.*, 2001). DEM has also been applied to simulate solid flows within the blast furnace (Zhou *et al.*, 2005). However, the cohesive zone was typically ignored or treated superficially, such as by reducing particle

size or by artificially consuming ore particles at a specified location. A previous attempt to simulate the softening-melting test using DEM (Chew *et al.*, 2004) focussed on structural rearrangement by reducing the stiffness of the particles and allowing large overlaps between soft particles (and conversely, small overlaps between hard particles). However, this was recognised as a very crude and limited representation as it did not allow for the physical shape change of the particles to be accounted for.

The aim of this work is to model the physical change that ore particles undergo during the softening-melting process. Recent studies (Kruggel-Emden *et al.*, 2008) have attempted to deal with non-sphericity in particles through the use of overlapping or intersecting spheres. There also has been significant progress in the simulation of agglomerates (including Thornton *et al.*, 1999 and Luding *et al.*, 2005). This work extends these approaches to develop a sub-particle DEM model, in which an agglomerate of smaller particles is used to represent a single macro particle. Rearrangement of the sub-particles within the agglomerate allows shape changes from deformation to be quantified.

The specific focus of this study is on the applicability of the force models used in DEM agglomerate models to the specific sub-particle approach proposed. Due to the large number of contact points within a realistic agglomerate (perhaps tens of sub-particles), it can be difficult to analyse any single contact's behaviour. Therefore, a limiting agglomerate of two sub-particles was used to inspect behaviour at the contact level. This approach allowed testing the dynamic response of the sub-particles under simple external force configurations. Direct verification that both the overall agglomerate and the contact point behave reasonably was the prime motivation. On this basis, the individual force formulations are evaluated so that a single formulation may be selected for further studies of full-sized agglomerates.

DISCRETE ELEMENT METHOD THEORY

Fundamental Basis

DEM solves Newton's second law of motion for individual particles (Cundall and Strack, 1979). Forces are calculated at contact points (particle-particle and particle-wall) in both the normal and tangential directions, and summed with those acting externally, e.g. gravity. The equations for conservation of momentum are then solved in the translational and rotational fields, as given in Equations 1 and 2.

$$m_i \frac{dv_i}{dt} = \sum F_{N,i} + \sum F_{T,i} + F_{G,i} \tag{1}$$

$$I_i \frac{d\omega_i}{dt} = \sum M_i \tag{2}$$

where m_i, I_i, v_i and ω_i are the mass, rotational inertia, translational velocity and angular velocity of the i-th particle, and $F_{N,}$ $F_{T,}$ F_G and M_i are the normal contact force, tangential contact force, gravitational force and moment of inertia calculated at each particle-particle and particle-wall contact.

The Verlet method as described in Allen and Tildesly (1987) is used to solve for the velocity and position of each particle at each time step.

Normal Force Models

There are two commonly used force models for DEM applications – linear and non-linear. Likewise with agglomerate models there have been two main approaches developed – Linear Hysteretic, which utilises different force constants for loading and unloading (Luding *et al.*, 2005), and the JKR method based on the Hertz non-linear model (Johnson *et al.*, 1971). Whilst both linear and non-linear models have been used successfully, there is often a trade-off between complexity of the model and accuracy of the results. As a result, both models have been used in this study to ascertain the applicability of each model to the present problem. Due to the complexity of implementing the JKR model a simplified version has been used accounting only for the surface energy effects and ignoring the effect of adhesion on the contact radius. In addition, a third model has been investigated, based on a linear spring model with a constant mass-based attraction force holding the particles together. A comparison between the force model equations used (Equations 3-9) is given in Table 1.

Table 1: Normal Non-adhesive and Adhesive Force Model Equations

Model	Non-adhesive Force	Adhesive Normal force
Hertz JKR (Johnson *et al.*, 1971)	$F_N = \frac{4}{3} E_{ij}^* \sqrt{R_{ij}^*}\, \delta^{\frac{3}{2}}$ (3)	$F_N' = F_N - \sqrt{4 F_N F_C}$ $F_C = 1.5\pi\Gamma R_{ij}^* \qquad \Gamma = \gamma_i + \gamma_j$ (4)

where F_N is the normal force, F'_N is the apparent normal force including adhesion, δ is the contact overlap , E^*_{ij} is the reduced Young's modulus for i and j, R^*_{ij} is the reduced radius for i and j, and γ_i, γ_j is surface energy of particle i, j.

Linear Hysteretic Luding *et al.* (2005)	$F_N = K_N \delta$ (5)	$F_N' = \begin{cases} k_1\delta & k_2(\delta-\delta_0) \geq k_1\delta \\ k_2(\delta-\delta_0) & k_1\delta > k_2(\delta-\delta_0) > -k_c\delta \\ -k_c\delta & -k_c\delta \geq k_2(\delta-\delta_0) \end{cases}$ (6)

where K_N is the normal linear spring constant, k_1, k_2 and k_c are the normal, adhesive and cohesive spring constants, and δ_0 is the equilibrium overlap of the contact. Note: k_2 is dependant on the historical maximum overlap ($\delta_{max,ij}$) of the contact up to a maximum (δ^*_{max}), as given below, where ϕ_f is the plasticity depth.

$$k_2 = k_1 + (k_{2,\max} - k_1)\frac{\delta_{\max,ij}}{\delta^*_{\max}}, \quad \delta^*_{\max} = \frac{k_{2,\max}}{k_{2,\max} - k_1} 2\phi_f R^*_{ij} \quad (7)$$

Linear Mass	$F_N = K_N \delta$ (8)	$F_N' = F_N - (m_i + m_j) * k_{adh}$ (9)

Where k_{adh} is the adhesion constant.

Tangential Force Model

The tangential model used in this DEM model is based on the widely accepted Mindlin and Deresiewicz model (Langston *et al.*, 1994). This is a two-stage rolling-sliding model, which is dependant on the total displacement of the contact point in the tangential direction, δ_t (Equation 10). If $\delta_t > \delta_{max}$, then sliding occurs and δ_t does not increase further. A tangential damping force is also calculated if the particle is not under sliding conditions.

$$F_T = -\mu_s F_N \left[1 - \left(1 - \frac{\min(|\delta_t|, \delta_{t\max})}{\delta_{t\max}} \right)^{3/2} \right] \hat{\delta}_t \quad (10)$$

where μ_s, δ_t, δ_{tmax} *and* $\hat{\delta}_t$ are the sliding friction coefficient, tangential displacement, maximum tangential displacement and unit contact vector in the tangential direction.

When using adhesive models, the contact force, F_N as calculated from the adhesive model can no longer be directly applied. This is due to two important phenomena from the adhesive component of the force – firstly F_N can be negative at displacements less than the equilibrium overlap, due to the attractive component of the adhesive forces. Secondly, the force is zero at a non-zero equilibrium overlap between the particles, however, in reality there can still be friction forces acting at this time. These issues have been discussed by Luding (2008) who proposed that for the Linear Hysteretic model the contact force used F_N can be replaced by (F_N - $k_c\delta$) when the force is attractive. A similar method has been proposed by Thornton and Yin (1991) for the Hertz JKR model that used an "effective" normal force for the calculation of the tangential interactions. In the model to be considered here, the normal force for a non-adhesive contact (Equations 3, 5 and 8) is used to determine tangential interactions for simplicity.

TWO-PARTICLE SIMULATIONS

An important feature of the sub-particle model is the ability to model plastic deformation of an agglomerate. The proposed model aims to do this through the re-arrangement of the sub-particles within the agglomerate. Since the sub-particles are represented by standard DEM interactions, it is worth noting how the normal and tangential forces are transmitted through an agglomerate via the contact points. By isolating a single contact point, the different formulations can be compared more easily. In all cases, gravity was ignored such that only the applied forces were active.

As multiple force models have been compared, equivalent variables needed to be chosen for the comparisons. Di Renzo and Di Maio (2004) have discussed the difficulty in selection of variable values by comparing the results of linear and non-linear force models. In this paper, the variables have been chosen to provide similar force curves for overlaps around and less than the equilibrium overlap, specifically the minimum force point corresponding to the applied force required to separate the particles. The parameters chosen are listed in Table 2. Soft particles were simulated in line with previous experimental work. A comparison of the force curves corresponding to the parameters is given in Figure 1, showing that each passes through the overlap $\delta = 2\text{x}10^{-4}$ m when $F'_N = 0$ (equivalent to 8% of the particle radius of $2.5\text{x}10^{-3}$ m).

Table 2: Parameters and conditions used for two-particle DEM simulations

Variable	Symbol	Value
Common		
Sub-particle radius	r_i	$2.5\text{x}10^{-3}$ m
Equilibrium overlap	δ_o	$2\text{x}10^{-4}$ m (8%)
Particle density	ρ	900 kg.m^{-3}
Time step	ΔT	$1\text{x}10^{-6}$s
Sliding friction coefficient	μ_s	0.4
Coefficient of restitution	ε	0.3
Linear Mass		
Linear Hysteretic		
Normal spring constant	k_1	$1\text{ x}10^3$ N.m^{-1}
Adhesive spring constant	k_2	$1.8\text{ x}10^3$ N.m^{-1}
Cohesion spring constant	k_c	$1.8\text{ x}10^3$ N.m^{-1}
Plasticity depth	ϕ_f	0.08
Hertz JKR		
Young's Modulus	E	$1\text{x}10^7$ kg.m^{-1}.s^{-2}
Poisson ratio	ν	0.23

Adhesion constant	k_{adh}	1700 $m.s^{-2}$	Surface Energy	Γ	15 $J.m^{-2}$
Normal spring constant	K_N	1 x10^3 $N.m^{-1}$			

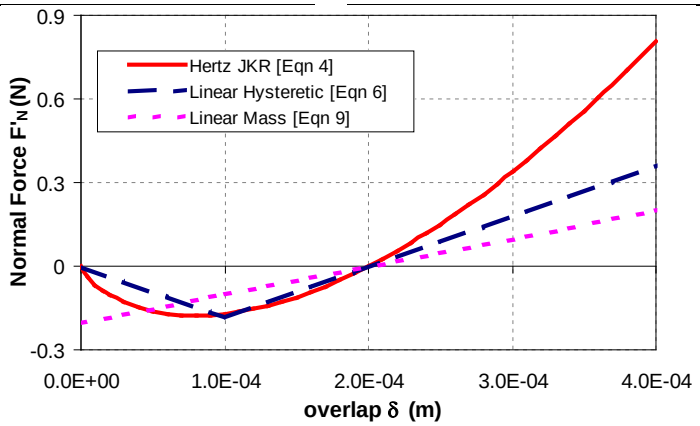

Figure 1: Comparison of force curves used in simulations

Results

In these simulations, two particles were created and a force applied to draw them together. Once attached, two external force configurations were investigated: 1) uni-axial tension until rupture separated the particles and 2) rotation of the agglomerate, initiated by equal forces in opposite directions applied to the particles perpendicular to the contact axis.

Uni-axial tension

An external force acting in a direction opposite to the contact vector was applied to each particle to test the separation behaviour of the agglomerate. Results showing the calculated stress from the applied force over the cross-sectional area of one of the particles against the strain on the agglomerate are given in Figure 2. In this figure, it can be seen that during separation the Linear Hysteretic and Hertz models both exhibit behaviour with an elastic limit above which fracture of the bond occurs. The only difference between these models is the slope of the stress-strain curve, with the Hertz model showing a non-linear slope compared to the linear response of the Linear Hysteretic model, as would be expected. For the linear mass model, the strain increases linearly with applied stress until rupture occurs, with the rupture point corresponding to the applied force equalling the attractive force. This simulation only shows elastic behaviour – no permanent deformation occurs from the applied force.

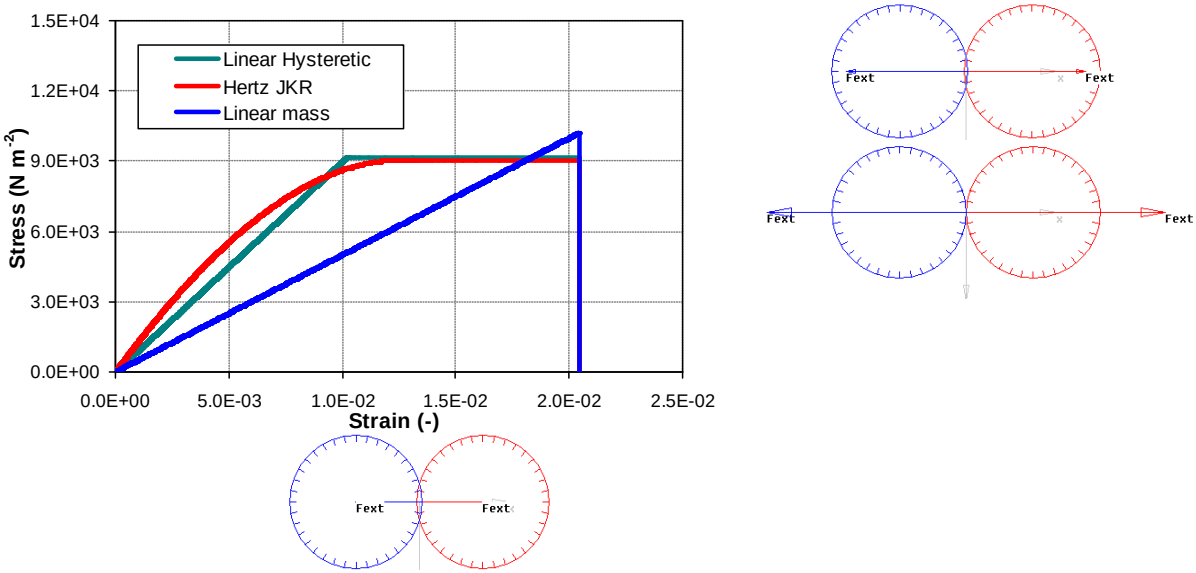

Figure 2: Stress-strain relationship during uni-axial tension

The Linear Hysteretic model appears to give a good piecewise approximation to the Hertz JKR model. The Linear Mass model would seem only able to represent brittle fracture type materials, as no parameter choice would affect the shape of its curve. For a realistically sized agglomerate, the behaviour required of a single contact is not yet quantified. However, the aim is to produce a model that is reasonable regardless of the number of sub-particles used.

Agglomerate rotation

To simulate the rotation of the agglomerate around its centre of mass, external forces are applied to each particle in opposite directions, perpendicular to the contact vector (as can be seen in Figure 3a). This creates a torque on the agglomerate that will cause it to rotate. Four behaviours were tested: 1) undamped oscillation, 2) damped oscillation, 3) pure sliding and 4) limited sliding. In the results discussed below the initially horizontal lines on the particles represent the initial contact vector from the centre of the particle to the contact point. This assists in visualising the degree of rotation of particles.

Undamped Oscillator

An undamped oscillator is mechanically equivalent to a continuous rod of material. Therefore, considering how tangential stresses are transmitted through the contact point, the necessary condition is that the tangential reaction force generated must be sufficiently stiff so as to not permit any significant displacement of the contact point, otherwise energy would be dissipated through the damping behaviour. Results for the undamped oscillation are given in Figure 4, which plots the linear displacement in the x-direction and the angular velocity of the red particles. It can be seen that the agglomerate oscillated with a period of 0.065 s, and this period remains constant over the simulation duration (30 periods). Results for the three formulations are overlaid showing indistinguishable behaviour.

Damped Oscillator

The behaviour simulated in a damped oscillator is that of a flexible rod of the same mass and rotational inertia as the agglomerate. In this system, the initial potential energy will be dissipated until the agglomerate is dynamically stable, oriented vertically with the external forces in line with the contact vector. In terms of the spring-dashpot model,

tangential displacement occurs through loading and unloading the spring, but is dissipated through the dashpot without exceeding the sliding limit (see Figure 3b). To satisfy these constraints, the contact conditions were softened indirectly by reducing the sliding friction coefficient ($\mu_s = 4\text{x}10^{-3}$), as shown by line (ii) in Figure 3c. Damped oscillator results are given in Figure 5. This damping can be seen to be different between the different force models, however it is of similar magnitude.

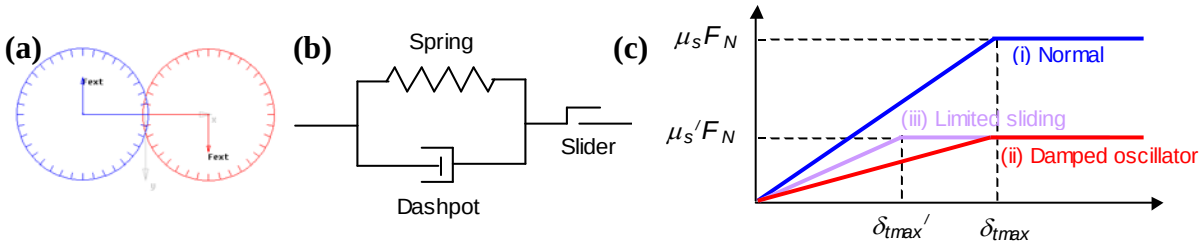

Figure 3: a) Initial position of agglomerate for rotation, b) Tangential spring-dashpot diagram, c) Tangential force-displacement relationship

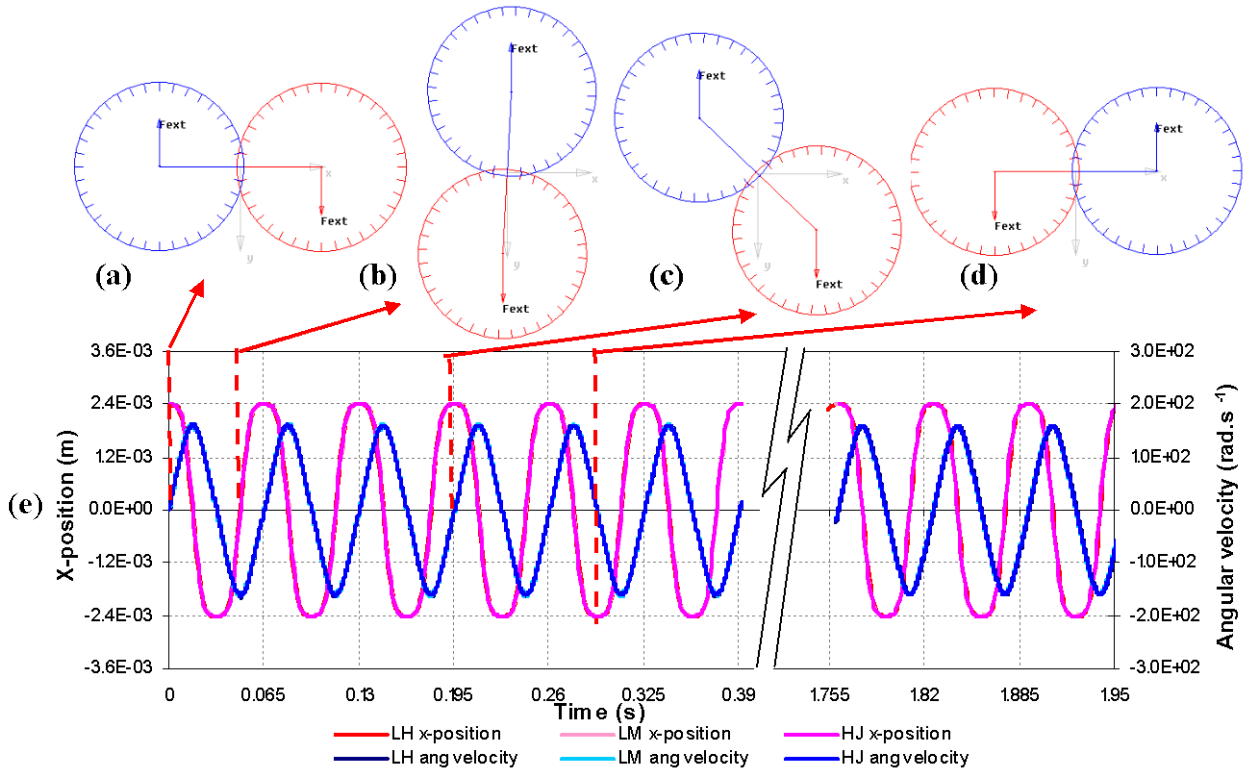

Figure 4: Results of agglomerate rotation simulation showing undamped oscillation – (a) to (d) position and orientation of particles, (e) x-position and angular velocity for Linear Hysteretic (LH), Linear Mass (LM) and Hertz JKR (HJ) models.

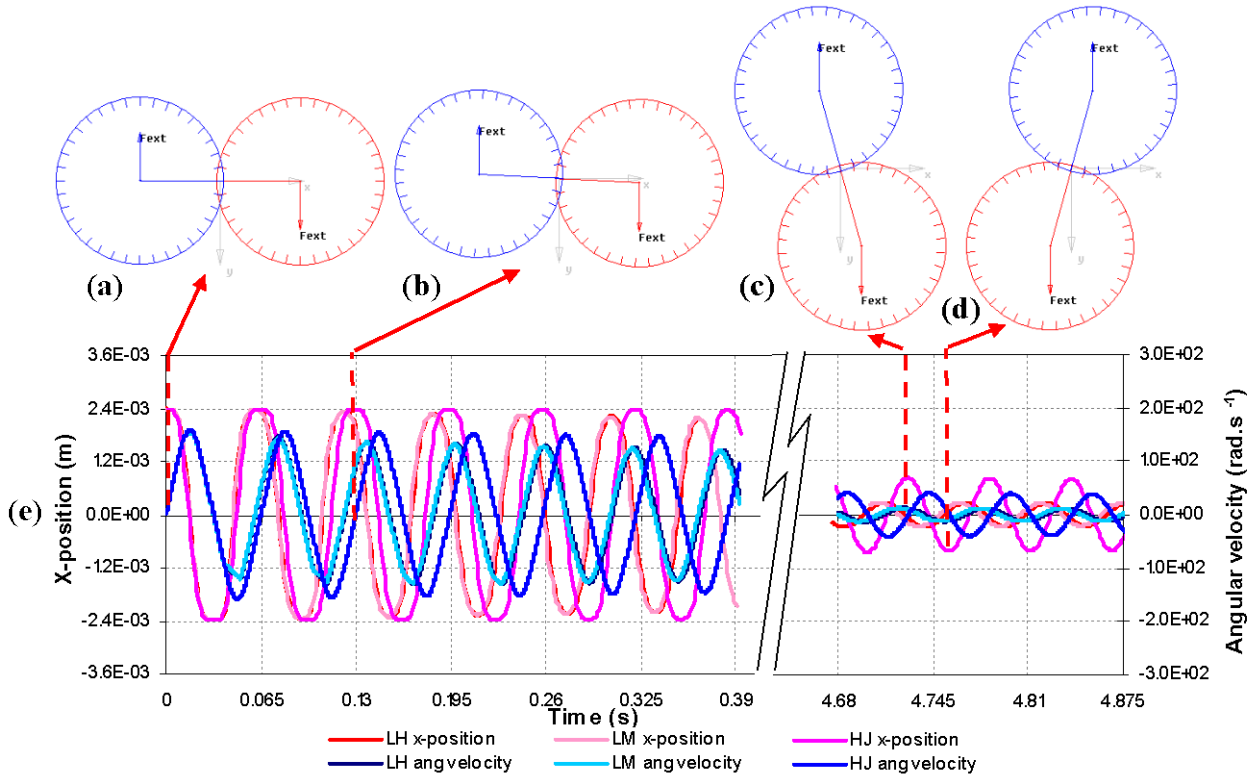

Figure 5: Results of agglomerate rotation simulation showing damped oscillation – (a) to (d) position and orientation of particles, (e) x-position and angular velocity.

Pure Sliding

The condition of pure sliding occurs when the tangential interactions are negligible compared to the normal interactions, thus to simulate this the sliding friction coefficient is set to zero. This simulates the particles moving freely around each other while remaining attached. The results (Figure 6) show that the agglomerate oscillates at a higher frequency (with a period of 0.0365 s) than in coupled rotation since the rotational inertia of the individual particles is significantly less than that of the agglomerate as a whole. The angular position of the particles remains constant throughout the simulation.

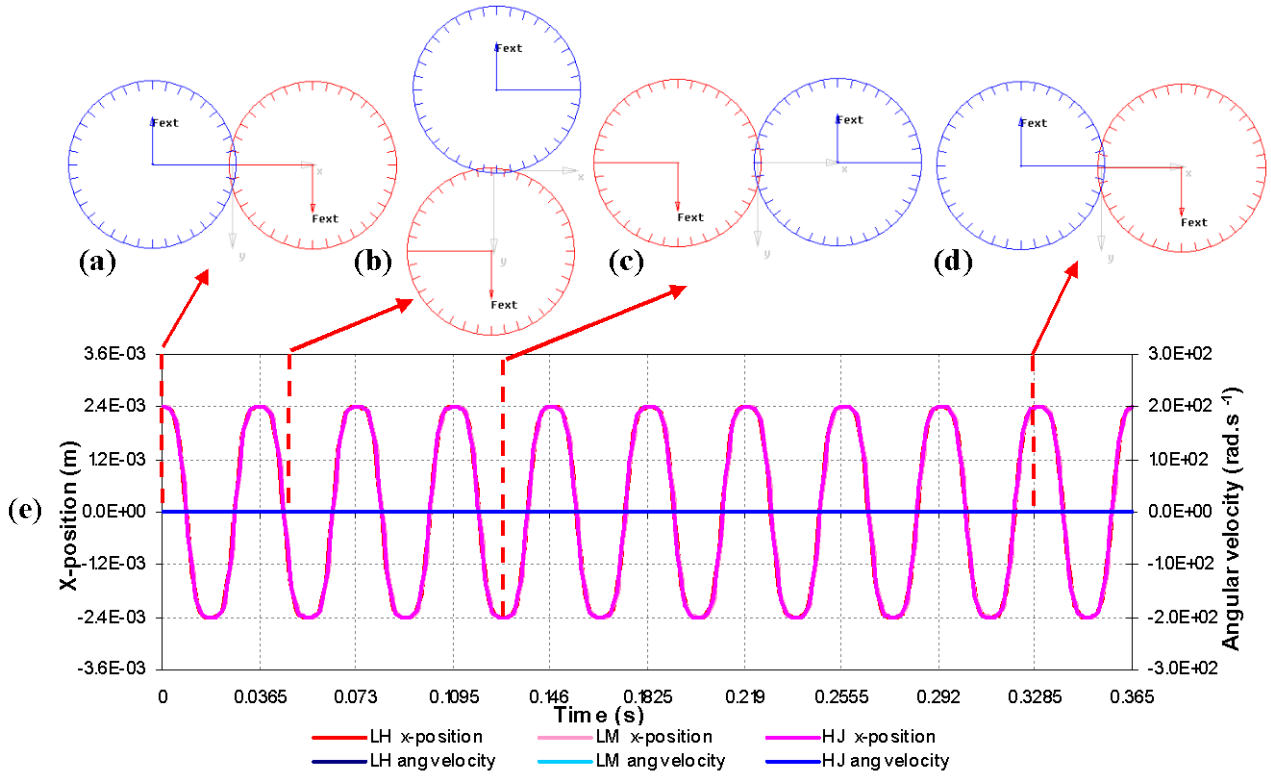

Figure 6: Results of agglomerate rotation simulation showing pure undamped sliding – (a) to (d) position and orientation of particles, (e) x-position and angular velocity.

Limited Sliding

The final case is an intermediate case with combined sliding and rotation. To achieve this, the maximum sliding overlap criterion (δ_{tmax}) is reduced and the sliding friction coefficient is decreased (μ_s = 4x10^{-4}), such that the limit for sliding is decreased (refer to line (iii) of Figure 3b).

Figure 7 shows the results for this case, indicating a highly damped oscillator. Initially, tangential displacement is stored in the spring until δ_{tmax} is reached. At this point (Figure 7a), the contact begins to slide, resulting in the straight sections of the angular velocity. At the position in Figure 7b, the rotation of the agglomerate has reached a maximum and the overall motion begins to reverse. At the contact point, this causes the spring to begin to unload, then load in the opposite direction, causing a sharp decrease in the angular velocity. Once the sliding limit is reached again, the curve again straightens, as sliding occurs. This process continues until sufficient dissipation has occurred to keep the system within the sliding limit and so the damped oscillator behaviour is recovered. However, the position of the contact point (Figure 7c and 7d) is now different from the initial conditions, representing plastic deformation.

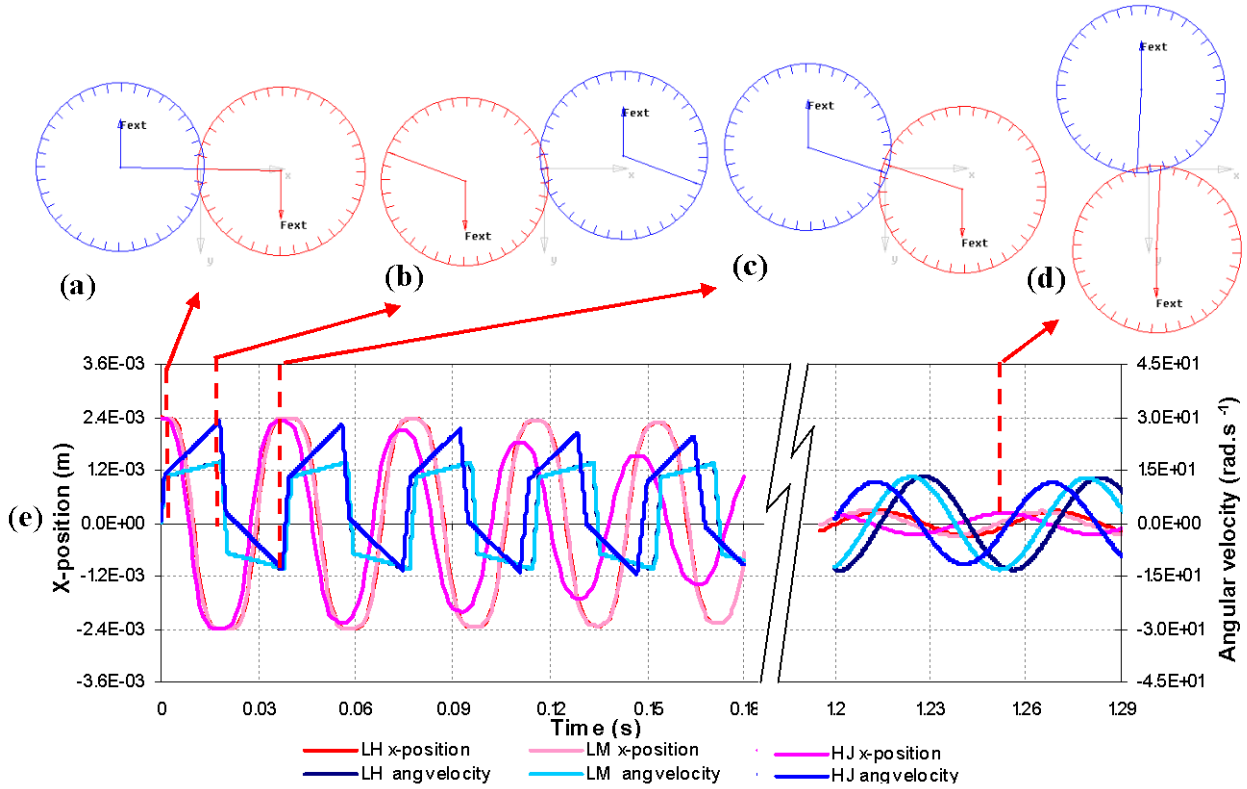

Figure 7: Results of agglomerate rotation simulation showing limited sliding – (a) to (d) position and orientation of particles, (e) x-position and angular velocity.

Discussion of Force Models

In general, the three force models produced similar results, due to the appropriate choice of variables. The Linear Hysteretic and simplified Hertz JKR models demonstrated soft separation behaviour in the uni-axial tension test; however, the Linear Mass model only replicated brittle fracture. Further work would be required to implement the full Hertz JKR model due to its complexity. All models were able to demonstrate the desired behaviour under rotation, with the only distinguishable difference being the magnitude of the dissipation occurring in the damped oscillator and the limited sliding cases. Consequently, none of the formulations studied is clearly superior, making the choice for a sub-particle model one of numerical convenience.

CONCLUSIONS

A DEM sub-particle model, where a single particle is represented by an agglomerate of sub-particles, has been developed to investigate macroscopic plastic deformation resulting from softening-melting of materials. A limiting agglomerate with two sub-particles was used to inspect behaviour at the contact point under uni-axial tension and in rotation. The force models have been shown to demonstrate both elastic and plastic behaviour as required, with similar results achieved from all of the force models. The sub-particle approach appears to be a promising method for simulating the shape change arising from deformation of particles due to softening and melting.

REFERENCES

Allen, M P, and Tildesley, D J 1987, *Computer simulation of liquids*, Oxford University Press.

Chew, S J, Zulli, P and Yu, A B 2001, 'Modelling of liquid flow in the blast furnace. Application in a comprehensive blast furnace model', *ISIJ International*, vol. 41, no. 10, pp 1122-1130.

Chew, S J, Zulli, P, Nightingale, R and Yu, A B 2004, 'Application of softening-melting test data in blast furnace', *Proc. 2nd International Conference on Process Development in Iron and Steelmaking*, Luleå, Sweden, 6-9 June, vol. 2, pp 405-416.

Cundall, P A and Strack, O D L 1979, 'A discrete numerical model for granular assemblies', *Geotechnique*, vol. 29, no. 1, pp 47-65.

Di Renzo, A and Di Maio, F P 2004, 'Comparison of contact-force models for the simulation of collisions in DEM-based granular flow codes', *Chemical Engineering Science*, vol. 59, no. 3, pp 525-541.

Johnson, K L, Kendal K and Roberts A D 1971, 'Surface energy and the contact of elastic solids', *Proceedings of Royal Society of London A.*, vol. 324, pp 301-313.

Kruggel-Emden, H, Rickelt, S, Wirtz, S and Scherer, V 2008, 'A study on the validity of the multi-sphere Discrete Element Method', *Powder Technology*, vol. 188, no. 2, pp 153-165.

Langston, P A, Tüzün, U and Heyes, D M 1994, 'Continuous potential discrete particle simulations of stress and velocity fields in hoppers: transition from fluid to granular flow', *Chemical Engineering Science*, vol. 49, no. 8, pp 1259-1275.

Luding, S, Manetsberger, K and Müllers, J 2005, 'A discrete model for long time sintering', *Journal of the Mechanics and Physics of Solids*, vol. 53, no. 2, pp 455-491.

Luding, S 2008, 'Cohesive, frictional powders: contact models for tension', *Granular Matter*, vol. 10, no. 4, pp 235-246.

Thornton, C and Yin, K K 1991, 'Impact of elastic spheres with and without adhesion', *Powder Technology*, vol. 65, no. 1-3, pp 153-166.

Thornton, C, Ciomocos, M T and Adams, M J 1999, 'Numerical simulations of agglomerate impact breakage', *Powder Technology*, vol. 105, no. 1, pp 74-82.

Zhou, Y C, Wright, B D, Yang, R Y, Xu, B H and Yu, A B 1999, 'Rolling friction in the dynamic simulation of sandpile formation', *Physica A: Statistical Mechanics and its Applications*, vol. 269, no. 2-4, pp 536-553.

Zhou, Z Y, Zhu, H P, Yu, A B, Wright, B, Pinson, D and Zulli, P 2005, 'Discrete Particle Simulation of Solid Flow in a Model Blast Furnace', *ISIJ International*, vol. 45, no. 12, pp 1828-1837.